Morphological and genetic characterisation of the root system architecture of selected barley recombinant chromosome substitution lines using an integrated phenotyping approach

Canto, C. De La Fuente; Kalogiros, D. I.; Ptashnyk, M.; George, T. S.; Waugh, R.; Bengough, A. G.; Russell, J.; Dupuy, L. X.

Published in:
Journal of Theoretical Biology

DOI:
10.1016/j.jtbi.2018.03.020

Publication date:
2018

Document Version
Peer reviewed version

Morphological and genetic characterisation of the root system architecture of selected barley Recombinant Chromosome Substitution Lines using an integrated phenotyping approach

C. De La Fuente Canto*[1,2], D.I. Kalogiros*[1,3,4], M. Ptashnyk[3], T.S. George[1], R. Waugh[1], A.G. Bengough[1,3], J. Russell[1] and L.X. Dupuy[1].

[1]The James Hutton Institute, Invergowrie, Dundee DD2 5DA

[2]School of Life Sciences, University of Dundee, Dundee DD2 1PP

[3]School of Science and Engineering, University of Dundee, Dundee DD2 1PP

[4] Current address, School of Mathematical Sciences, University of Nottingham, Nottingham, NG7 2RD

* These authors contributed equally to this study and are both considered as primary author

Correspondance: L.X. Dupuy, lionel.dupuy@hutton.ac.uk

ABSTRACT

Discoveries on the genetics of resource acquisition efficiency are limited by the ability to measure plant roots in sufficient number and adequate genotypic variability. This paper presents a root phenotyping study that explores ways to combine live imaging and computer algorithms for model-based extraction of root growth parameters. The study is based on a subset of barley Recombinant Chromosome Substitution Lines (RCSLs) and a combinatorial approach was designed for fast identification of the regions of the genome that contribute the most to variations in root system architecture (RSA). Results showed there was a strong genotypic variation in root growth parameters within the set of genotypes studied. The chromosomal regions associated with primary root growth differed from the regions of the genome associated with changes in lateral root growth. The concepts presented here are discussed in the context of identifying root QTL and its potential to assist breeding for novel crops with improved root systems.

Key words: rootphenotyping, QTL, barley, RCSL, growth parameters, computer assisted breeding

INTRODUCTION

Profitability in modern agriculture relies heavily on the supply of water and fertiliser to maximise crop yield (Boserup, 2005). The current agro-economic model is now under increased scrutiny not only because of the damage it causes to the environment (Secchi et al., 2007), but also because of its possible vulnerability to climate changes (Letter et al., 2003) and the increasing cost and scarcity of some of the mineral compounds used in fertilisers (White et al., 2012). Reducing the dependency of modern agriculture on water and fertilisers is a major undertaking, and it has been proposed that breeding programs should now focus on the development of crop varieties that are more efficient at capturing the soil resources (Lynch, 2011).

To date, the genetic improvement of crops for improved resource acquisition efficiency has proved challenging. A plant acquires water and mineral elements from the soil through a system of interconnected roots, the arrangement of which we refer to as the Root System Architecture (RSA). The RSA is a complex object for breeders and geneticists to comprehend and utilise. The length and topological arrangement of roots within the RSA is dynamic because growth and lifetime of individual roots is controlled by a combination of developmental, physiological and environmental signals perceived by the plant (Bingham et al., 2010; Forde and Lorenzo, 2001; Wilkinson and Davies, 2002). The development of RSAs is also very stochastic (Forde, 2009) and statistical characterisation of root traits and growth parameters usually requires large replication numbers (Adu et al., 2014), observations in soil are destructive and labour intensive (do Rosario et al., 2000), and *in vivo* measurement techniques are partial (Nagel et al., 2012). Some progress has been achieved in the understanding of genetic control of RSA and its potential for breeding. For example recently, a QTL controlling root growth angle in rice, Deeper Rooting 1 (*DRO1*), has been characterised and cloned (Arai-Sanoh et al., 2014; Uga et al., 2013). Nevertheless, major constraints for genetic studies in RSA persist. Because root traits are greatly affected by the

environment, their heritabilities in many cases are low compared to shoot traits (Courtois et al., 2009). Although genotypic variability is found for root traits in controlled conditions, and QTLs have been identified, very few have been translated and used routinely in breeding (de Dorlodot et al., 2007; Sandhu and Kumar, 2017). QTLs should generally be validated in field conditions before using a marker assisted selection (MAS, Comas et al., 2013) but root traits measured *in vivo* are not always directly related to field performance. Hence, root QTL studies face limitations that need to be overcome through improved approaches able to dissect the genetic control of relevant RSA parameters for the development of more efficient crops.

There is great hope that technological development in root phenotyping systems could overcome some of these challenges. Traditionally, root phenotyping is achieved in the field using either soil coring or shovelomics. Soil columns are extracted from the field, roots contained in the soil columns are washed, and usually image analysis software is used to measure total root length in the sample (Watt et al., 2005). More recent shovelomics methodology relies on field measurement of the crown roots of the plant to describe parameters such as root gravitropism (Trachsel et al., 2011). These methods provide root data grown in their natural environment, but the measurements are destructive and time consuming. Non-destructive methods are a preferable approach to study roots (Downie et al., 2015). Mini-rhizotron tubes can be placed in the soil to observe roots *in situ* in undisturbed soils (Cai et al., 2016; Rewald and Ephrath, 2012); Laboratory-based rhizotron boxes allow part of the root system to be observed through glass windows (Nagel et al., 2012) with monitoring of root growth for long periods of time and image acquisition can be automated; X-ray computed tomography allows *in situ* imaging of soil cores of a range of size (Mooney et al., 2012), and various artificial media systems for phenotyping are being developed (Clark et al., 2011; Downie et al., 2012; Topp et al., 2013).

Techniques to analyse the data produced by phenotyping systems are not advancing at a comparable rate. What appears to be a limiting factor is the ability to process data, derive quantitative information on the growth and developmental processes of plant roots and understand

how these are genetically controlled. In this paper, we propose a new framework where processing of phenotypic data is tailored to the genetic material, here a set of barley Recombinant Chromosome Substitution Lines (RCSLs, Matus et al., 2003). We produced data using germination paper phenotyping system commonly used in the community (Gioia et al., 2017; Le Marié et al., 2014; Thomas et al., 2016), and developed mathematical modelling techniques to obtain chromosomal regions that are related to changes in the dynamic root growth parameters.

MATERIAL AND METHODS

Plant material

Five barley genotypes were chosen from a set of Recombinant Chromosome Substitution Lines (RCSLs, Fig. 1). The RCSLs were derived from an initial cross between a cultivated parent (cv. Harrington) and a naturally drought tolerant wild donor from the Fertile Crescent as described previously (Matus et al., 2003). Selection of the sub-set of genotypes was based on a previous assessment of the impact of drought on yield across two growing seasons during field trials (De La Fuente Canto et al, unpublished). Contrasting lines were selected: OSU044 and OSU048 showed a poor to moderate but stable yield across water treatments (stable RCSLs); OSU144 and OSU052 produced large yield potential in favourable conditions, but under drought their yield was significantly reduced (sensitive RCSLs); and finally, cv Harrington was chosen as control elite variety for the RCSLs and OSU060 as a line whose performance was intermediate and similar to the performance of cv. Harrington.

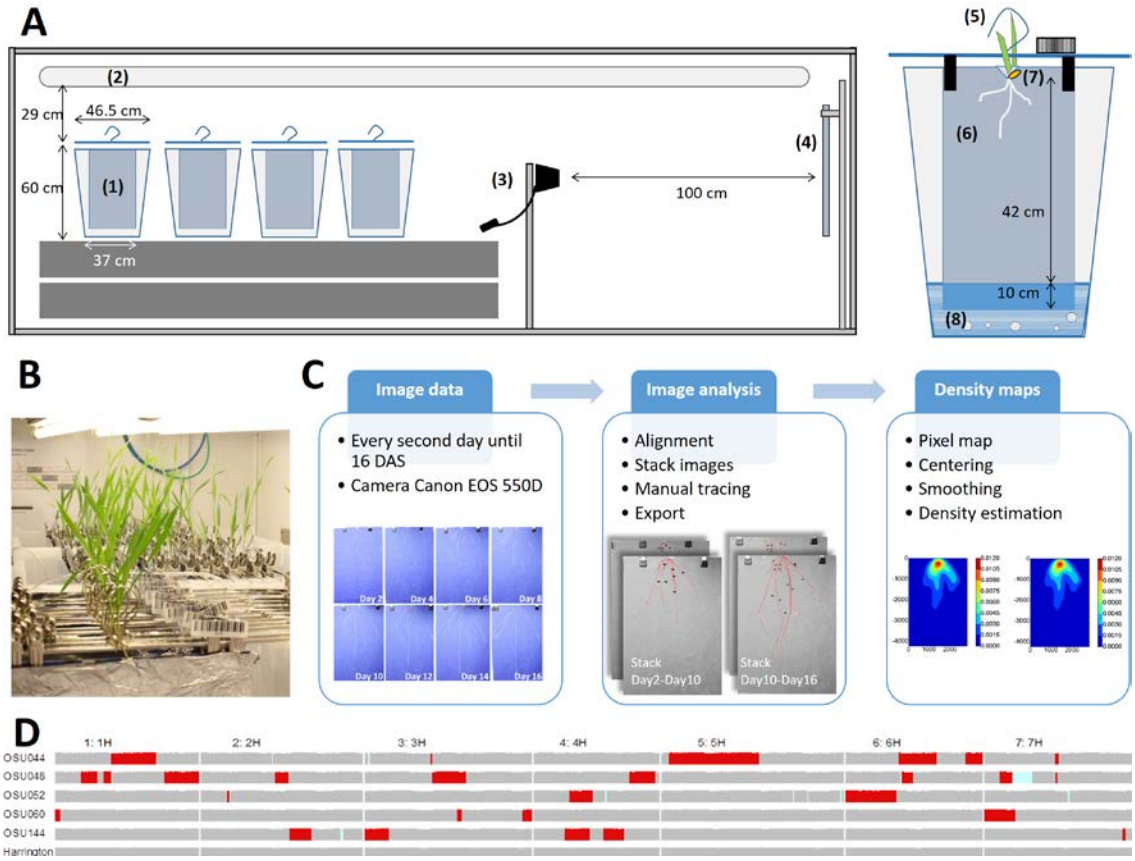

Figure 1. *The root phenotyping study. A) Diagram of the pouch-and-wick experimental setup used to grow barley seedlings under controlled conditions. (1) Each bucket contained two experimental replicates (12 seedlings, one per plate). (2) Lighting consisted of fluorescent tube light placed at 29 cm above the buckets and (3) a Canon EOS 550D camera was used for image acquisition. The camera was placed on a tripod with a remote shutter-release attached. (4) An artists'easel was used to hold the samples at a reference position and (5) the clip hangers used to hold the samples on the easel were fitted with a barcode. (6) Roots grew on A3 size clear-Perspex plate and acetate sheet with blue germination paper in between. Each plate was wrapped in foil and (7) seedlings were attached in a slit on top of the germination paper. (8) The nutrient solution was aerated with a pneumatic pump and 10 cm of the germination paper was submerged in nutrient solution. B) Picture of the experiment in the growth room. C) Diagram of the data processing framework. The raw phenotyping data consisted of images taken every two days for 15 days after sowing. The images were analysed using a series of steps including registration for aligning data with a reference image, stacking, tracing and exporting the pixel ROI data to files. Pixel ROI data were*

then used to generate root density distribution maps for primary and lateral roots. This was done using kernel-based density distribution methods combined with a centering of the data with respect to the midpoint of the horizontal plane (position of the slit on the germination paper). D) Graphical representation of the genotypes of the 5 RCSLs used in the study and cv. Harrington. Dark red areas indicate the introgressions from the wild parent and light grey areas indicate the modern background. Missing marker data are indicated in light blue. Each chromosome is oriented with the short arm from the left.

Experimental system

Plants were grown in a controlled environment in a 2D pouch and wick system (Hund et al., 2009; Liao et al., 2001). To avoid contamination during experiments, seeds with uniform size were surface sterilized by a vapour-phase sterilisation method using 100 ml sodium hypochlorite 4.5% and 5 ml concentrated HCl. The seeds were placed in opened Falcon tubes and treated for an hour with chlorine fumes inside a desiccator jar placed in a fume hood. Sterilised seeds were sown on 10x10 cm germination paper (Anchor Paper, St. Paul, MN, USA) moistened with sterile distilled water, placed in Petri dishes and maintained vertically in a Qualicool™ cooled incubator for two days at 20°C with no light. The equipment used for the experiments, e.g. buckets, plates and acetate sheets, was thoroughly washed first in bleach and subsequently in ethanol. Three days after sowing (DAS), seedlings of similar size were transferred to large sheets of germination paper (29.7 x 52 cm) pre-soaked with the nutrient solution, described below. Seedlings were held on the germination paper between an A3 size clear-Perspex plate and a 240 micron thick acetate sheet.

Each germinated seed was placed in a slit at the top of the germination paper and glued to the plate with a drop of diluted Solvite wallpaper paste (Henkel Limited, Winsford Cheshire, UK). The germination paper was placed between a plate and an acetate sheet and held with two foldback clips attached on the sides and a clip hanger at the top. Each sample was then wrapped in

aluminium foil to protect the roots from light and suspended into plastic boxes (60 cm x 68 cm x 46.5 cm) containing 30 L of nutrient solution into which only approximately 10 cm of the germination paper was submerged (Fig. 1). The nutrient solution was constantly aerated with a pneumatic pump and changed every four days.

The same nutrient solution was used to soak the germination paper and to fill in the plastic containers. The nutrient solution was prepared with deionized water and contained 300mM NH_4Cl, 400mM $Ca(NO_3)_2$, 400mM KNO_3, 300mM $MgSO_4$, 100mM FeEDTA, 1M KH_2PO_4, 6mM $MnCl_2$, 23mM H_3BO_3, 0.6mM $ZnCl_2$, 1.6mM $CuSO_4$, 1mM Na_2MoO_4, 1mM $CoCl_2$. The pH was adjusted to 5.5 at the start of the experiment using NaOH and the nutrient solution was replaced every four days. Eight replicates of each genotype were distributed in four plastic boxes, two complete replicates per box. Plants were grown for 15 days in a growth room under a 16/8 h day/night cycle at a constant temperature of 15ºC and 60% relative humidity approximately. Average light intensity during the day hours was 80 μmol m^{-2} s^{-1} at plant height.

Phenotyping system

1. Image acquisition

Pictures of each plate were taken every two days from day 2 to day 16 of the experiment with a Canon EOS 550D camera fixed on a tripod set on autofocus mode at a distance of 1 meter from the germination paper. The plate was hung in an easel with a 1 m working distance. The aluminium foil and acetate sheet were removed for taking pictures and, before putting them back, the germination paper was sprayed with approximately 1ml of the nutrient solution to ensure a homogeneous diffusion of the nutrients in the root system growing media and avoid mineral deficiency towards the end of the experiment.

2. Harvest

After the last image, 18 day-old seedlings were removed from the plates. Shoots were excised from the roots and fresh weight of the shoots was recorded. Roots were detached from the germination paper and stored at room temperature in 50% ethanol until scanning. A reference picture of the final root system was acquired in high resolution (400dpi) using an Epson Expression 10000XL professional DIN A3 scanner (Seiko Epson Corporation, Japan). Analysis of scanner images were performed with WinRHIZO (Regent Instruments, Quebec, Canada) to collect data on average root diameter and total root length at harvest. Shoots and roots were dried at 60 °C for 72 hours before determining dry weight (DW).

3. Image processing

Image data were analysed through manual tracing of individual root trajectory using a liyama ProLite T2735MSC touch screen and Fiji software (Schindelin et al., 2012). Raw images were first transformed into 8-bit grayscale images. For each genotype, the elongation rate of seminal and lateral roots as well as the branching rate of seminal roots were analysed on two time-steps, from day 2 to day 10 and from day 10 to day 16 of growth. Tracing was obtained using the freehand tool for several reasons. Automated tracing tool requires manual adjustment due to variation in the background or difficulty to detect small roots (Leitner et al., 2014; Lobet et al., 2011; Pound et al., 2013), and the majority of lateral roots were too short to gain benefit from automation. Also, the analysis does not require topology but just length distribution and the time gained by automated tracing is offset by the requirement to connect seminal roots with laterals. ROI (Region Of Interest) files produced for seminal and lateral roots of all the replicates for each genotype were then processed by a custom macro so that the pixel coordinates of all roots in the images were exported in text files.

Tracking of individual roots in coarse time lapse automatically is not easy, and often not possible when roots are grown in soil. We propose,instead, to determine growth parameters directly from changes in total root length and total root numbers during the course of the experiments. Such estimates can be obtained because in the absence of mortality there is a direct relationship between

elongation rate, branching rate, total number of roots and total root length. The relationship was proposed by Hackett and Rose (1972) and it can be transformed to derive root growth parameters:

$$e^{(0)}(t) = \frac{l^{(0)}(t+dt) - l^{(0)}(t)}{n^{(0)}dt}$$
$$b_r^{(0)}(t) = \frac{n^{(1)}(t+dt) - n^{(1)}(t)}{dt - T} \quad (1)$$
$$e^{(1)}(t) = \frac{2l^{(1)}(t+dt) - l^{(1)}(t)}{n^{(0)}b_r^{(0)}(dt-T)^2}.$$

Here, $e^{(0)}(t)$ and $e^{(1)}(t)$ (cm d^{-1}) are the elongation rate for, respectively, the seminal and lateral roots and $b_r^{(0)}(t)$ (d^{-1}) is the branching rate of lateral roots. The parameter *dt* indicates the duration of the examined growth interval of 8 days (day 2 to day 10) and 6 days (day 10 to day 16) respectively, while $l^{(0)}(t)$ (cm) and $l^{(1)}(t)$ (cm) are the total seminal and lateral root length at time *t*, respectively. The number of seminal roots is denoted by $n^{(0)}(t)$, the total number of laterals is denoted by $n^{(1)}(t)$. Since the number of seminal roots for the replicates of each genotype increased with time, $n^{(0)}$ was taken as the mean number of seminal roots during a given time interval where growth parameters were determined. For lateral roots, there was a time delay between the emergence of the first appeared seminal and the emergence of lateral roots. The parameter *T (d)* is therefore the time it takes for lateral roots to emerge from the primary root. In this experiment, it applied only to the first time step (day 2 - day 10), since after 8 days, laterals had emerged from all primary roots. *T* was evaluated as the mean value of the time delay observed among the replicates of a single genotype.

The rate at which the angle of the root changes towards verticality (termed gravitropic rate) was determined using stacked images from day 2 and day 4. Images were first registered (alignment of the base of the root system) using the plugin Align Image by line ROI (Schindelin et al., 2012). Registration of images used the top and bottom of the slit as common feature to perform alignment across the different images of a given plant. Two types of angles were recorded for these images. First the angle of the root with the vertical axis (α) was measured at day 2 using the Straight Line ROI. In this setting, α is 0 when the root is vertical. Then, the change in angle ($d\alpha$) taking place for

the same root between day 2 and day 4 was determined as the angle between the two segments of root (between day 2 and day 4) using Segmented Line ROI and angle measurement. Three randomly selected seminal roots of each plate were measured. The root gravitropic rate parameter ($g^{(0)}$) is defined as the relative decrease in vertical angle per unit time and it was determined for each genotype using the information gathered for a total of 24 seminal roots as follows:

$$g^{(0)}(t) = \frac{\alpha(t) - \alpha(t + dt)}{\alpha(t)dt} \quad (2)$$

where *dt* is equal to 2, since the change in angle was measured for an interval of 2 days.

4. Genetic analysis

A scoring system termed Combinatorial Quantitative Trait Loci (C-QTL) is proposed to visualise the effect of exotic introgressions on the root growth parameters measured during the experiments. The algorithm exploits the genomic structure of the introgressions and processes markers by blocks during the analysis. An algorithm is then designed to score each block of markers. The algorithm selects two groups of genotypes and considers blocks of markers that vary between and within the groups of genotypes and adds to or substracts from the score based on phenotypic differences. The process is repeated for all possible groups of genotypes to provide an overall score for each block of markers.

Formally, the C-QTL score from the set of plants phenotypes φ^i is derived from the genetic composition G^i of a genotype. The genetic composition of the ith plant is defined as $G^i = \{g_1^i, g_2^i, \dots g_n^i\}$ with i ≤ s (number of blocks), such that g_k^i takes the value 0 if the kth block of markers is that of the elite line and g_k^i takes the value of 1 if the kth block of markers is that of the exotic line. The ith genotype is also defined by its phenotype φ^i which is the quantitative trait corresponding to the genetic make up G^i. We therefore assume genotypes and phenotypes are related according to the following probabilistic model:

$$P(\varphi^i < x) = \int_{-\infty}^{x} N\left(x - a^i - \sum_{k \le n} b_k g_k^i, \sigma\right) dx \quad (3)$$

where φ^i is considered to be normally distributed so that $N\left(x - a^i - \sum_{k \le n} b_k g_k^i, \sigma\right)$ is the Gaussian function of mean $x - a^i - \sum_{k \le n} b_k g_k^i$ and standard deviation σ. Here a^i is the mean trait value observed on the modern variety, b_k is the effect of the i[th] marker on the genotype, σ is the standard deviation of the residual, and N is the Gaussian distribution function. If two groups of distinct genotypes U_1 and U_2 are obtained, then variations between and within groups can be exploited to score each region of the genome using the following formula:

$$D_k^{1,2} = \delta_k^{1,2}\left(\frac{1}{n_1}\sum_{i \in U1} \varphi^i - \frac{1}{n_2}\sum_{j \in U2} \varphi^j\right), \quad (4)$$

$$E_k = \sqrt{max_{r=1,2}\left(\frac{\gamma_k^r}{n_r}\left(\sum_{i \in Ur} \varphi^i - \varphi^r\right)^2\right)} \quad (5)$$

where γ_k^r=1 if there exists two genotypes P_i and P_j in U_r such that $g_k^i \neq g_k^j$ and $\gamma_k^r = 0$ otherwise. E_k is therefore an estimate of the standard error of the mean within groups of genotypes.

Since there are many possible groupings on which to carry out such analysis, a logical and computationally efficient way to process the entire dataset is to use a clustering algorithm to group genotypes based on their similarity and to cumulate the indicators D_k and E_k on the possible set of clusters identified. The following formula is therefore obtained for scoring individual markers:

$$I_{C-QTL} = \left\{\frac{1}{n_{clusters} - 1}\sum_{k=3}^{k \le n_{clusters}}\left[\frac{1}{{n_{clusters}}^2 - n_{clusters}}\left(\sum_{i,j \le n_{clusters}} D_k^{i,j}\right) - E_k\right]\right\}. \quad (6)$$

C-QTL analysis was run for all four root growth parameters: the elongation rate of seminal root $e^{(0)}$, the elongation rate of lateral roots $e^{(1)}$, the branching rate $b_r^{(0)}$ and the gravitropic rate $g^{(0)}$ (the rate at which the angle of the root changes towards verticality). The data were transformed so

that the value of each of these growth parameters had zero mean and variance equal to 1. Clusters were created using the Agglomerative Clustering from the Scikit library (Pedregosa et al., 2011).

5. Description of the change of the root system over time using a time-delay density based model

Direct estimation of root growth parameters from an experimental dataset is often problematic. It requires tracking and measuring the growth of single roots at different time points. It is time consuming at best and not possible when partial observations are made, for example in rhizotron systems. The Hackett and Rose (1972) approach allows direct estimation of growth parameters in bulk and remove the need for tracking individual roots, but it lacks a true spatial formalism. It does not provide ways of estimating parameters such as gravitropic rate, branching angle or responses to spatial heterogeneity, and results of direct estimations are sensitive to missing data (Kalogiros et al., 2016). Hence, we propose a model that extends Hackett and Rose (1972) approach to include the spatial distribution of roots. Because both space and time are considered, the model was generalised into a set of partial differential equations including both time and space derivatives and also requiring more sophisticated numerical techniques to derive the growth parameters

The mathematical framework proposed to build on the work presented in Kalogiros *et al.* (2016) where root systems were modelled as a continuum and changes in the architecture of the root system over time were mathematically described with time-delay partial differential equations. The initial model was extended so that it could be used to extract growth parameters from time-lapse data. Modifications included time-varying growth parameters to characterise the changes in growth patterns over time, enabling the time delay in the emergence of lateral roots to be consistent with the time-lapse data considered in order to facilitate the spatial and temporal evolution of RSA.

Root density distributions are functions depending on the horizontal distance (x), depth (y) and root angle (α), which was defined with respect to the vertical axis. Therefore, at any point (x, y, α) the number of root tips per unit volume changes according to the main conservation equation:

$$\frac{\partial \rho_{\mathrm{a}}^{(i)}}{\partial t} + \nabla \cdot \left(e^{(i)} \rho_{\mathrm{a}}^{(i)} \left(\sin \alpha \, , \cos \alpha \, , -g^{(i)} \alpha \right) \right) = b^{(i)}, \text{ with } i \geq 0 \quad (7)$$

The index (i) describes the type of root so that seminal roots are denoted with the index 0 and lateral roots are denoted with the index 1. The root tip density is denoted by $\rho_{\mathrm{a}}^{(i)}$ (cm^{-2}) and $\frac{\partial \rho_{\mathrm{a}}^{(i)}}{\partial t}$ is the change with respect to time of the root tip density. The operator $\nabla \cdot$ is the divergence with respect to the independent variables x, y, α and $e^{(i)}(t)$ $(cm\, d^{-1})$, $g^{(i)}(t)$ (d^{-1}) and $b^{(i)}(t)$ $(cm^{-2} d^{-1})$ describe respectively the elongation rate, gravitropic rate and the volumetric branching rate (termed also "branching rate" in the following sections) as functions of time. Since only seminal roots emerged from the base of the root system during the experiment, $b^{(0)} = 0$. For lateral roots, the branching rate is non zero and is specified as

$$b^{(i)}(x, y, a, t) =$$

$$\frac{1}{2} b_r^{(i-1)} \left[\rho_{\mathrm{a}}^{(i-1)} \left(x, y, \alpha + b_a^{(i)}, t - T^{(i)} \right) + \rho_{\mathrm{a}}^{(i-1)} \left(x, y, \alpha - b_a^{(i)}, t - T^{(i)} \right) \right], \quad (8)$$

with $i \geq 1$,

where $T^{(1)}$ *(d)* is the time delay observed before the emergence of the first appeared 1st order lateral root, $b_r^{(i-1)}(d^{-1})$ is the seminal root branching rate and $b_a^{(i)}$ is the branching angle. In this setting, the root length density distributions $\rho_l^{(0)}$ and $\rho_l^{(1)}$ are derived from the root tip density distribution as $\int e^{(0)}(t)\, \rho_{\mathrm{a}}^{(0)}$ and $\int e^{(1)}(t)\, \rho_{\mathrm{a}}^{(1)}$, respectively. Numerical solutions for Eqns (7) and (8) were obtained using an upwind finite volume solver with minmod flux limiters.

6. Spatial and temporal mapping of the root system architecture using density functions

In the next stage, the root tracing data were transformed into root length density so that model predictions could be compared directly to experimental data. The lists of pixels describing root trajectories (ROI) were first processed to extract lists of root segments, their spatial coordinates, the length of the segment and its angle. Length density distribution functions were then determined using a kernel-based density estimation method. The method followed the principles of Kalogiros et al. (2016) but in this study, it was applied to pixel data directly and at different times during the experiment (day 2, day 10 and day 16). Kernel functions were fitted on data by the adjustment of

the band width *k* of the kernel function. A Gaussian function was used to obtain smooth representation of the densities and facilitate fitting of solutions of the model to the data. The heterogeneity of the distribution of root segments in space is a main challenge in order to achieve a good fit, because the data point distribution is dense along a root and sparse between roots. In this case, it is advantageous to consider groups of segments belonging to a single root (V-fold grouping) and apply cross validation to these groups of roots instead of separate random data points (Kalogiros et al., 2016).

In a time-lapse dataset, both the number of root segments and the volume explored by roots increase with time. These two factors have an opposite effect on the optimal *k*, with a higher number of segments lowering *k* values and a larger explored volume increasing *k* values. Overall, *k* values always increase because the number of points increase linearly with time, but the explored volume increases more rapidly as a power function of time. In order to simplify the analysis, we choose the largest optimal value of *k* which was always on the last day of growth. Hence, the bandwidth *k* was first evaluated on the last day of the experiment (day 16) and the same value was used for estimating the root length density for the other time points of the experiment. Finally, the seminal root length density distribution maps on each day were aligned with respect to the midpoint of the horizontal distance of the plane (Fig. 1; Step C).

7. Estimation of time-dependent model parameters from time-lapse data

The Hackett and Rose (1972) approach allows direct estimation of root growth parameters (Eqn 1) because the model can be inversed analytically to provide simple formula for growth parameters. This is not the case in general for fitting the currently presented model to experimental data . Instead, simulation algorithms must be used to find optimal parameters that best describe the series of experimental observations. With these stepwise algorithms (described formally below) the model is first initiated with the root density distribution at day 2of the experiment. Subsequently, an error function must be defined to quantify the difference between observed and modelled root length density. A minimisation algorithm then provides the best set of parameters to move from the

initial condition to the next step of the experiment. This procedure is repeated for the different growth increments recorded during the experiment.

Here, the length density was initiated directly using the kernel-based density estimation. Since it is not possible to distinguish between root tips and root bases from the tracings, the length density at day 2 was also used to determine the root tip density, as follows:

$$\rho_a^{(0)}(x,y,\alpha,2) = n^{(0)} \frac{\hat{\rho}_l^{(0)}(x,y,\alpha,2)}{\int \hat{\rho}_l^{(0)}(x,y,\alpha,2)dxdyd\alpha} \quad (9)$$

with $\hat{\rho}_l^{(0)}$ denotes the root length density distribution function estimated using kernel-based methods from the experimental data made available on day 2. The same data wereused to determine the initial value of the root length density at the beginning of the numerical simulation of the model. The optimal set of growth parameters was obtained using the following robust error function $E^{(i)}$:

$$E^{(i)} = \int_V \hat{\rho}_l^{(i)^2} \left(\rho_l^{(i)} - \hat{\rho}_l^{(i)}\right)^2 dxdyd\alpha + \left(\int_V \left(\rho_l^{(i)} - \hat{\rho}_l^{(i)}\right) dxdyd\alpha\right)^2 \quad (10)$$

The first integral term accounts for local differences between the observed $\hat{\rho}_l^{(i)}$ and predicted $\rho_l^{(i)}$root length density. It is a modification of the mean square error that reduces the dependency of the error on areas of relatively low root length density in the spatial domain. The second term of the error accounts for the differences in the total root length density. The Nelder-Mead optimisation algorithm was used to obtain the parameter values $e^{(0)}$ and$g^{(0)}$. Lateral root growth parameters $b_r^{(0)}$ and $e^{(1)}$were obtained in a second stage.

Model fitting was carried out stepwise, with each experimental time increment treated as a distinct optimisation sub-problem. Both the model parameters and the root densities (root length and root tip density) were initiated from those obtained from the previous sub-problem. To insure stability of the simulations, the time increment of simulations was fixed to the smallest admissible increment for all the sub-problems determined from the Courant–Friedrichs–Lewy condition. To

maintain a constant grid size, the bandwidth *k* of the density estimation was determined on the last time-step of the experiment (largest *k* value for each genotype).

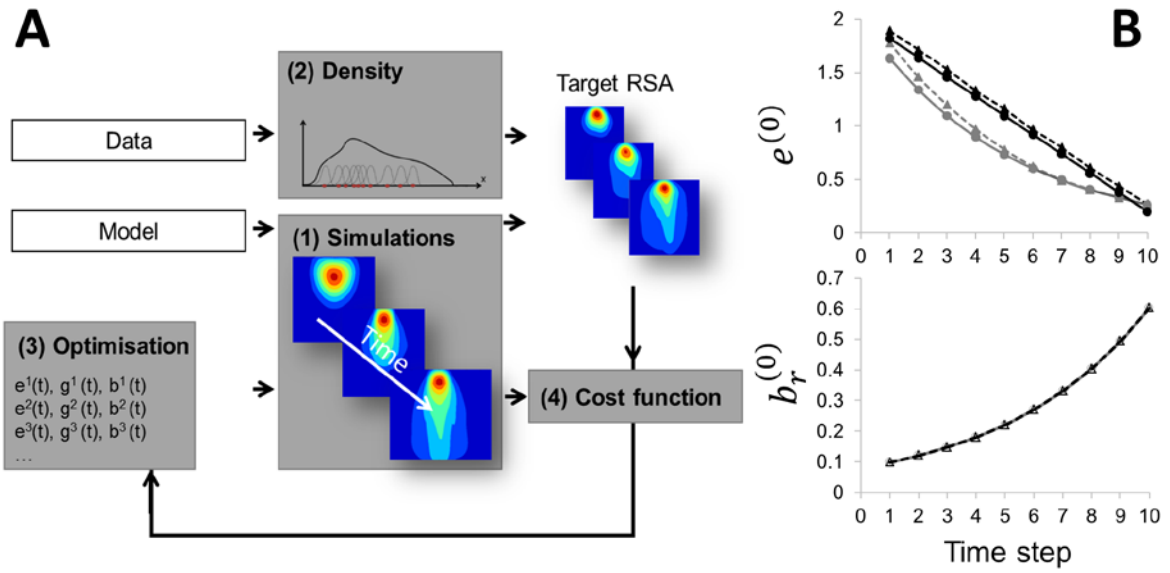

Figure 2. *A) Diagram of the optimisation process for automatic identification of growth parameters over time. The target root system architecture (RSA) at specific time points results from the available experimentally observed time-lapse data or artificial data (model-generated data with model parameters known). A target root length density distribution function is derived from simulations with user-defined time-varying parameters for each time step (1) so that it is feasible for the estimated model parameters to be directly compared with target parameters over time. When dealing with experimental data, root density estimation methods (2) are applied to obtain the target RSA. Then, the optimal time-dependent model parameters are determined by applying a minimisation algorithm (3) that proposes, at each time step, a set of new candidate model parameters. The new set of parameters is then used in a simulation and the results of this simulation are compared with the target root system using a cost function (4). The optimiation procedures (3 and 4) are iterated until a convergence criterion is met. The output seminal root distributions with the estimated optimal parameters at a specific time step are used as the initial condition for the evaluation of the optimal model parameters at the next time step. B) The quality of the fit obtained with the optimisation algorithm was tested on simulated data using time-varying elongation rate and branching rate. In the top figure, the imposed elongation rates (linearly or*

exponentially decreasing with time) are drawn using plain lines and those retrieved by the optimisation algorithms are drawn in dashed lines. Additionally,in the bottom figure, the imposed branching rate is drawn using plain lines and those retrieved by the algorithms using dashed lines.

First, the parameter extraction pipeline was benchmarked on simulated data for which growth parameters were known. The model used to establish the benchmark consisted of Eqns (7) and (8), for which the elongation rate $e^{(0)}$ was either a linearly decreasing function of time or exponentially decreasing function of time and the branching rate $b_r^{(0)}$ increased exponentially with time. The data generated by these models were used in the optimisation algorithm described above and the results were compared with the model parameters used to generate the target root length density function. In the second step, the optimisation algorithm was applied to the entire root tracing dataset (Fig. 2). For each time interval the Model Elasticity Value (MEV) of the error was determined as the percentage increase in the error induced by a 1% increase in each model parameter. Confidence intervals for model parameters were estimated using the V-fold bootstrap method proposed in Kalogiros *et al (*2016).

8. Software for numerical simulations and statistical analysis

Numerical simulation of the model equations and parameter estimation was performed using the Python programming language (Python Software Foundation. Python Language Reference, version 2.7. Available at http://www.python.org). The algorithms were implemented in the Python SciPy library (http://www.scipy.org/) using a personal computer of 3.1 GHz CPU (IntelCore i5-2400 CPU @ 3.1 GHz) and 4 Gb RAM. We provide software and code for simulation and estimation of growth parameter from root tracing data under the BSD and GNU General Public License. The modules provided include a) the numerical algorithm for root simulation of root growth (Main.py), b) algorithms for estimation of length density mappings from experimental data (Roots_VFold_CrossValidation.py) and c) algorithms for the extraction of growth parameters from experimental data (Optimisation.py). All the programs can be downloaded at

http://archiroot.org.uk/tools/model-based-phenotyping.html. Statistical analysis of the genotypic effects on root traits was performed using a two factorial mixed model considering the genotype, the time-step (day 2 to day 10, day 10 to day 16 of the experiment) and their interaction as fixed effects. The experimental replicate was considered as the random effect. Genstat 17th Edition (VSN International, UK) was used for this analysis.

RESULTS AND DISCUSSION

Integrated phenotyping and computational methods allow automated extraction of growth parameters

The phenotyping system based on germination paper was tailored for the observation of barley roots of up to 18 days-old and image acquisition using a DSLR camera. After fifteen days of growth, seminal roots fitted tightly within the boundaries of the A3 sized pouches, without touching any of the edges. Similar phenotyping systems have been successfully used in cereal crop plants such as maize (Hund et al., 2009), wheat (Atkinson et al., 2015) and brassica species (Adu et al., 2014; Thomas et al., 2016). The preparation of samples and room temperature during growth allowed good control of contamination from fungi and algae with no significant contamination observed after 18 days of growth. Elongation rate of seminal roots (approximately 1 - 2.5 cm d^{-1}) was similar to those measured in soil (Dupuy et al., 2010; Valentine et al., 2012), in hydroponics (Rose, 1983) or in gels (Shelden et al., 2013). Visual inspections of the plant showed vigorous growth and no signs of stress and mineral deficiencies. Other simple phenotyping systems have been used in the past e.g. gel chambers (Bengough et al., 2004), imaging at the surface of transparent cylinders (Kristensen and Thorup-Kristensen, 2004) or gel systems (Topp et al., 2013), but cost and the time for sample preparation in such systems is higher. Although the study focused on few selected genotypes, results showed the phenotypic pipeline is suitable to detect genotypic variations in rooting traits, and similar analyses could be carried out on larger number of genotypes

simply by allowing for more pouches to be grown simultaneously during an experiment. This has been achieved in a recent study on Brassica genotypes (Thomas et al., 2016).

Our approach to the analysis of root data included manual operations to handle the samples and analyse the images, with about one minute required to trace an entire root system. However, Various software and techniques are now being developed to automate the analysis of root images. Robots are being used to acquire image data automatically (Nagel et al., 2012) and root tracing algorithms (Armengaud et al., 2009; Lobet et al., 2011; Pound et al., 2013) can be used to obtain descriptions of the root system and its topology. Recent developments made in computer vision also indicates there is a great potential for new software to remove most manual interventions from image processing. Techniques could for example combine root tip detection (Kumar et al., 2014) with optimal path search (Pound et al., 2013), active contour (Makowski et al., 2002), or tracking algorithms (Mairhofer et al., 2012). However, the development of automated image analysis techniques may unleash large quantity of complex root data for which there is currently no method or strategy to process and analyse. In particular, it has proved particularly difficult to derive meaningful growth parameters from root growth data when only parts of the root system is visible (Dupuy et al., 2010; Garré et al., 2012). Research presented here shows that mathematical models of root systems provide a useful framework to perform such tasks, applicable on various plants and different types of experimental systems including rhizotrons (Kalogiros et al., 2016).

Mathematical models allow accurate estimation of time varying growth parameters

Optimisation techniques have been used for model calibration (Reddy and Pachepsky, 2001) to predict, for example, the spread of roots through soil under different fertilisation regimes (Heinen et al., 2003). The problem of extracting biologically meaningful information from data is more challenging because models can make accurate predictions including parameters with no biological significance. Recent attempts to solve this problem have shown that root growth rates can be

estimated accurately when the root system is simple (Kalogiros et al., 2016), but when more complex models are used the optimisation process is more challenging (Garré et al., 2012) .

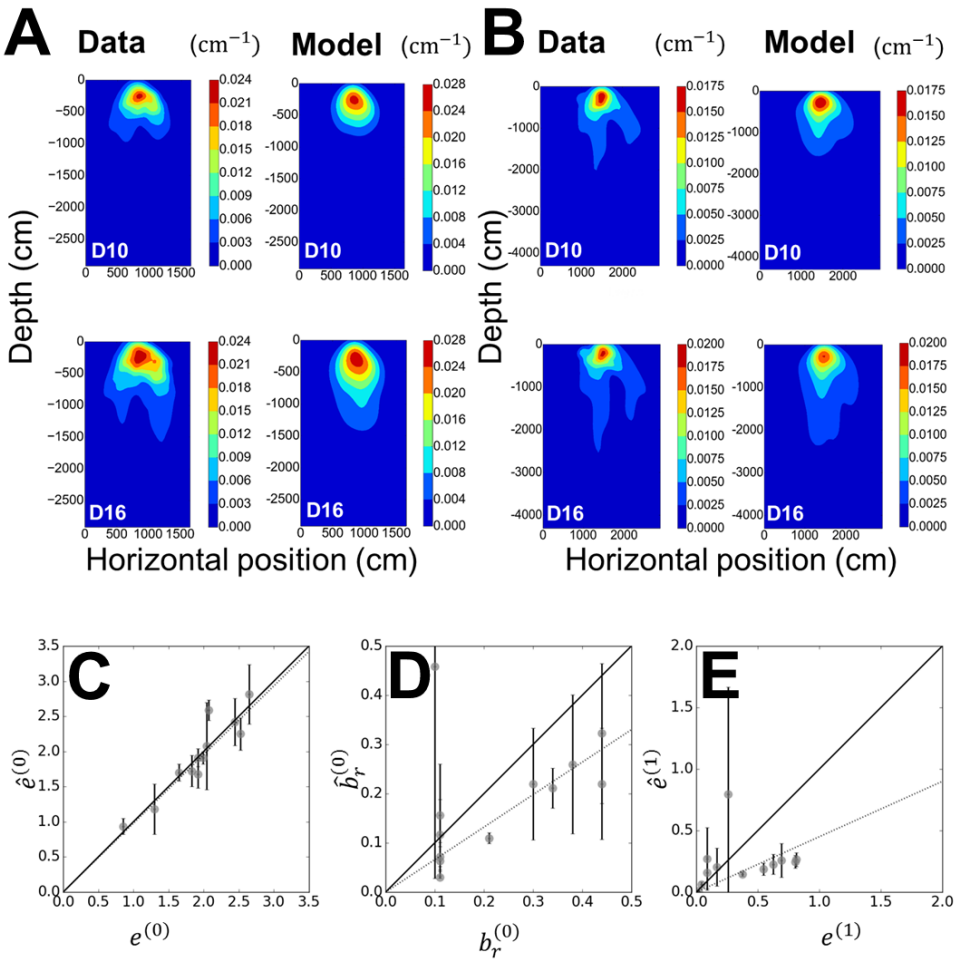

Figure 3. *Comparison between data and model predictions. After the optimisation process, root length density estimation matched the experimental data at Day 10 (D10) and Day 16 (D16) of the experiment. The data is presented for A) genotype OSU 048; and B) genotype cv. Harrington. Differences between model and data arise from the non-smooth variation in root length density due to limited number of genotypes. Overall quality of the extraction of growth parameters (C-E) was assessed by plotting the direct estimate with the model-based growth parameters for the entire dataset (all time steps and genotypes). Results show good estimation of elongation rate of primary roots* $e^{(0)}$ *(C) The branching rate* $b_r^{(0)}$ *(D) and the elongation rate* $e^{(1)}$ *of lateral roots (E) could also be predicted but with less accuracy due to the variability of the growth rate of lateral roots. Plain lines indicate 1:1 relations and dotted lines show differences in model predictions.*

The difficulty of extending optimisation of model parameters to time varying parameters and time lapse data is that parameters of the numerical algorithm for model simulation such as grid size, time increment or the size of the data buffer for simulation of delays are dependent on both the duration of growth and the observed root system through the bandwidth *k* of the kernel estimator.

Genotype	**Elongation** $(cm \cdot d^{-1})$		**Gravitropism** (d^{-1})		**Total root length**(cm)		**Predicted total root length**(cm)	
	Δt_1	Δt_2	Δt_1	Δt_2	Δt_1	Δt_2	Δt_1	Δt_2
OSU_048	0.85	1.30	0.258	0.224	68.30	107.42	68.91	108.72
OSU_044	1.92	1.99	0.168	0.162	109.83	164.92	110.83	166.99
Harrington	2.04	1.83	0.167	0.174	137.48	201.00	136.72	201.35
OSU_060	2.07	1.65	0.178	0.190	137.42	196.01	136.46	195.95
OSU_052	2.44	1.92	0.174	0.174	152.49	214.54	154.46	217.49
OSU_144	2.65	2.52	0.155	0.129	161.56	242.58	159.86	242.46

Table 1. *Estimated root growth parameters for primary roots using the optimisation pipeline (Fig. 2) and comparison between measured and predicted total root length.*

Genotype	**Branching** (d^{-1})		**Elongation** $(cm \cdot d^{-1})$		**Total root length**(cm)		**Predicted total root length**(cm)	
	Δt_1	Δt_2	Δt_1	Δt_2	Δt_1	Δt_2	Δt_1	Δt_2
OSU_048	0.383	0.109	0.690	0.260	13.52	37.27	13.42	37.05
OSU_044	0.207	0.114	0.373	0.017	3.59	4.37	7.33	8.27

Harrington	0.442	0.110	0.806	0.087	11.71	20.54	11.52	20.45
OSU_060	0.296	0.110	0.548	0.086	7.07	13.40	7.00	13.67
OSU_052	0.444	0.114	0.814	0.044	7.99	11.91	5.82	9.71
OSU_144	0.337	0.104	0.624	0.168	6.47	19.05	5.37	18.83

Table 2. *Estimated root growth parameters for lateral roots using the optimisation pipeline (Fig. 2) and comparison between measured and predicted total root length.*

Assessment of the performance of our method was carried out visually through comparison of the experimental root length density distributions with the predicted root length density distributions. (Fig. 3 A-B). The growth parameters obtained on the experimental data were also compared with direct measurements (Fig. 3 C-E, Table 1 and 2). Strong correlations were observed between direct measurements of growth parameters and model based estimations of those parameters. All correlations were significant ($p<0.001$). Model predictions were greater for the elongation of seminal roots. The elongation rate had a coefficient of variation varying between 5% and 20%, and there was little bias with overestimation of the predictions by a factor of 1.03 (Fig. 3C). The growth of lateral roots was more stochastic with a coefficient of variation for the branching rate ranging between 9%-94% and for the elongation rate between 20% and 110%. This variability affected considerably the predictions. The branching rate of lateral roots was overestimated by a factor of 1.5 (Fig. 3D). The elongation of laterals showed the weakest model predictions which were obtained with an over estimation by a factor of 2 (Fig. 3E). Likewise, the gravitropic rate was more difficult to determine experimentally due to the stochasticity of the direction of growth. Direct estimation of gravitropic rate was obtained using the angle of primary roots at day 2 and day 4. However, there was a strong correlation between the initial angle of the root and the magnitude of the change in the angle ($p<0.001$, with average R^2 of 0.59). This confirmed the linearity of the gravitropic response as was proposed in earlier theoretical studies (Dupuy et al., 2010). However, this measure of the gravitropic rate may be of limited value because it was obtained at a fixed point

in time. The measure is therefore more sensitive to root stochasticity and it may not be representative for the overall plant behaviour since the gravitropic rate may change with time. Results suggest that the global estimation of the gravitropic rate using the optimisation pipeline was more realistic (Table 1). Direct estimation of the gravitropic rate predicted genotype OSU060 to be more gravitropic than cv. Harrington whereas they were genetically and visually very similar (Fig. 4). There was no major difference in the estimates of the gravitropic rate obtained from the optimisation pipeline for the duration of each growth period between genotypes.

Both genotypic and temporal factors affect root growth parameters

Recombinant Chromosome Substitution Lines with contrasting response to drought in field trials showed remarkable genotypic variations in the morphology of their root system at early growth stages. Seminal root elongation rate was the most discriminating variable across the RCSLs ($p<0.001$, Table 3). For instance, OSU048 (stable but limited yield performance) had a remarkably low and uniform elongation rate throughout the experiment (0.94 ± 0.04 cm d^{-1} and 1.13 ± 0.14 cm d^{-1} from day 2 to 10 and from day 10 to 16 respectively, Fig. 4). In contrast, OSU144 (sensitive but large yield potential) showed an overall decrease in elongation rate for the seminal roots, with a higher elongation rate from day 2 to 10 (2.8 ± 0.2 cm d^{-1}) than from day 10 to 16 (2.3 ± 0.1 cm d^{-1}). This trend was observed for all genotypes except OSU048 and OSU044. Branching rate and lateral root elongation rate showed large variation at the genotype level due to the stochasticity of these growth parameters. For all the genotypes, the number of lateral roots emerged from day 2 to day 10 of the experiment was larger than the number of lateral roots that emerged from day 10 to 16. Genotypic differences were found for elongation rate of lateral roots ($p<0.05$, Table 3). Lateral roots in OSU048 grew vigorously from day 10 to 16 (0.7 ± 0.3 cm d^{-1}) and this resulted in a much larger total lateral root length at the end of the experiment (40.2 ± 7.0 cm), compared to genotypes such as OSU044 (4.5 ± 1.4 cm) and OSU052 (13.3 ± 3.5 cm) which had a lateral root growth rate that was significantly lower (Fig. 4). OSU048 and OSU144 were the two most contrasting phenotypes with a final total root length of 159.4 ± 10.7 cm and 284.5 ± 23.8 cm respectively. OSU060 was selected because of the similarity of its performance to cv. Harrington in field conditions (de La

Fuente Canto, in preparation), and results showed its growth parameters were comparable to cv. Harrington (Fig. 4). This suggests the exotic introgressions present in OSU060 also had a negligible effect on the root system at this stage of development.

Trait	Genotype	Time	Genotype x Time-step
Lateral roots number	ns	***	ns
Lateral total length	*	***	**
Log_lateral_tot_length	ns	***	*
Branching rate	ns	***	ns
Lateral elongation rate	ns	*	ns
Log_lateral_elong_rate	*	ns	**
Seminal roots number	ns	ns	ns
Seminal elongation rate	***	***	***

Table 3. *Analysis of the genotype and time effect on root parameters using a mixed effect model. Statistical significance (p-values) are provided for the fixed effects using a chi-squared based Wald-test using residual maximum likelihood (REML). Level of significance is provided for (*) $p<0.05$; (**) $p<0.01$; and (***) $p<0.001$.*

Overall, these results indicate that introgressions of exotic DNA in the genetic background of a modern barley can have a strong effect on root system architecture at establishment stage. Although the link between response to water deficit and root system architecture is not demonstrated in this study, there are multiple indications that modern agriculture and the heavy supply of water and fertiliser to crops have led to significant changes in the size and architecture of root systems (Letter et al., 2003). This was illustrated in comparative studies of modern and ancient crop varieties (Chloupek et al., 2006). In barley, modern cultivars were found to have larger numbers of seminal roots with a wider angular spread of roots compared to their wild relatives

553 (Bengough et al., 2004). To engineer crops that are efficient in low input cultivation conditions, it
554 is probable that the roots of such new crops will need to acquire soil resources from different
555 regions of the soil. For example, improving the rooting depth could be used for resistance to
556 drought (Kato et al., 2006) and enhanced lateral root development in the topsoil could provide
557 better phosphorus uptake efficiency (Lynch and Brown, 2002; White et al., 2013).
558
559 Although few genotypes were screened in this study, there was strong evidence of genotypic
560 variations in root growth parameters of the RCSL population. This result shows the potential of
561 exotic allelic variation in the modification of root system architecture of modern barley cultivars.
562 For example, there was significant variation in root gravitropism and primary root elongation rate
563 between the RCSL genotypes, and this could be exploited to create deep rooting genotypes. Del
564 Pozo et al. (2012) found evidence suggesting segregation in the deep root phenotype within the
565 RCSL population used for this study. The authors carried out a field trial and found that drought
566 tolerant RCSLs had greater values of grain $\Delta^{13}C$ compared to cv. Harrington, which may indicate
567 greater access to soil water during grain filling and a more extensive root system (Tambussi et al.,
568 2007). The differences found for root elongation rate and gravitropism at early stages of
569 development in the RCSLs tested in the present study support this hypothesis since these two traits
570 have been associated with deep rooting phenotype in cereal crops (Araki et al., 2002), and they
571 have been shown to be an important quantitative trait to improve water uptake and yield under
572 water stress in rice (Uga et al., 2013) and maize (Hund et al., 2009). There were also significant
573 variations in the elongation rate and branching rate of lateral roots. Lateral roots are essential to the
574 acquisition of nutrients because they allow intensive exploration of the soil between the main root
575 axes and because of their ability to solubilize minerals adsorbed on the surface of soil particles.
576 Lateral roots for example, have been shown to increase the uptake of immobile nutrients such as
577 phosphorus (Lambers et al., 2006).

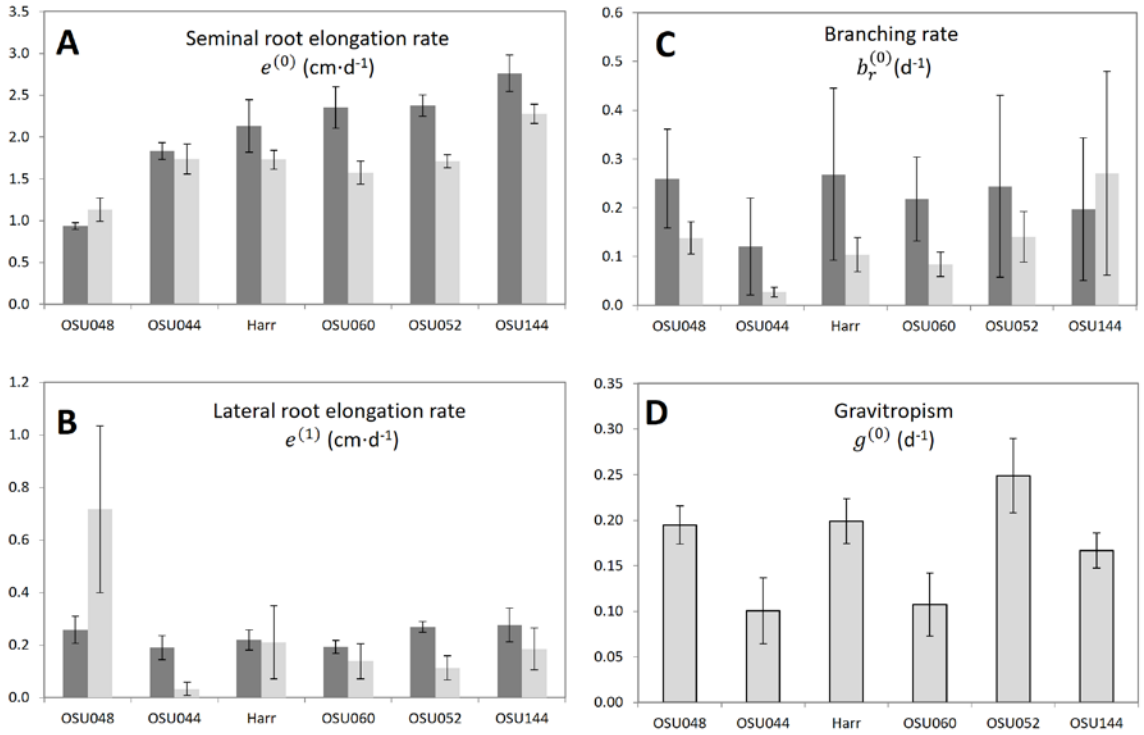

Figure 4. *Variations in root growth parameters with time and as a function of genotype. Bar charts represent mean values (+/- SE) for A) seminal root elongation rate (cm* d^{-1}*); B) lateral root elongation rate (cm* d^{-1}*); C) branching rate (*d^{-1}*). Growth parameters from Day 2 to Day 10 are plotted with dark grey shading, and growth parameters from Day 10 to Day 16 is plotted with light grey shading. D) Genotypes' mean value for gravitropic rate measured from Day 2 to Day 4. Error bars represent standard error of the mean.*

Analysis RCSLs phenotypic data

The genomes of Recombinant Chromosome Substitution Lines (RCSLs) are characterised by substitutions of entire blocks of the genome with the DNA of an ancient variety (RCSLs, Matus et al., 2003). Because the region of DNA inserted are quite large, a much-reduced number of lines is sufficient to induce variations over the entire genome. This is particularly appealing to root genetic studies where phenotyping is particularly time consuming, and this could be used, for example, to exclude quickly regions of limited influence on rooting trait. However, it is unclear how best to analyse the phenotypic data of such genetic material to derived useful knowledge on the genetics of root growth. Traditional QTL mapping analysis such as the composite interval mapping (CIM)

595 used by Uga et al. (2013) in 117 rice RILs or the multiple interval mapping (MIM) used by Chen et
596 al. (2010) in a 134 F_4 barley mapping cannot be applied directly.
597
598 In this study, we proposed a combinatorial approach (C-QTL) to quantify the phenotypic effects of
599 blocks of markers. The method allows visualisation of the influence of ensembles of markers that
600 covary in the selection of lines employed in the study. The method makes group of lines and
601 compute a score for each group of marker, using variations observed between and within groups.
602 Since there are different ways of grouping genotypes, a cluster algorithm was used to create the
603 sets of relevant groups on which the metric was cumulated. Since the metric accounts for both
604 within group variability and between group variability, it emphasize regions of the genome that
605 were linked to the largest variations in a quantitative trait, but also the regions on which no
606 information can be derived.
607
608 The C-QTL method described here is inspired from techniques used in non-parametric statistics.
609 For example, bootstrapping uses random resampling of the data with replacement to produce
610 simulated data of how an estimate varies, and to compute confidence intervals of estimates directly
611 from these simulations (Efron and Tibshirani, 1994). Cross validation techniques employ a range
612 of resampling schemes (leave-one-out, leave-p-out, V-fold, Monte Carlo) for example to determine
613 the log likelihood of a model (Burman, 1989). In a permutation test, samples are randomly
614 rearranged between groups to assess the likelihood of the null hypothesis (Kim et al., 2000). The
615 method also shares some similarities with single marker mapping (Geldermann et al., 1985) since
616 the metric determined on two sets of genotypes is a direct estimate of the effect of the group of
617 markers that makes the two groups genetically different. However, the C-QTL approach is
618 different from these methods, in that the whole dataset is used in the simulations and it is the
619 grouping of the data that is resampled to compute the net effect of a marker. Intuitively, the method
620 provides an optimal way of grouping genotypes that minimises the number of computations while
621 maximises the information contained in the metric.
622

The method was tested on a larger selection of RCSL lines using heading date as a reference trait and results can be access on Zenodo repository (de la Fuete Canto, 2018). The test showed C-QTL co-locate with key genomic regions associated with barley phenology (de la Fuete Canto, 2016). To date, however, it is unclear how the resampling of the groups affects the bias and variance of the estimators of the marker effect, and how different ways of grouping genotypes could improve the quality of the estimates. Additional theoretical work is now required to further characterise the mathematical properties of C-QTL estimates. Further development could also expand the technique to include common statistics on the significance of the effects of markers. For example, permutation tests could be implemented in the C-QTL analysis to determine the statistical significance of the QTLs identified (Doerge and Churchill, 1996), because they do not require *a priori* knowledge of the statistical distribution of the sample data.

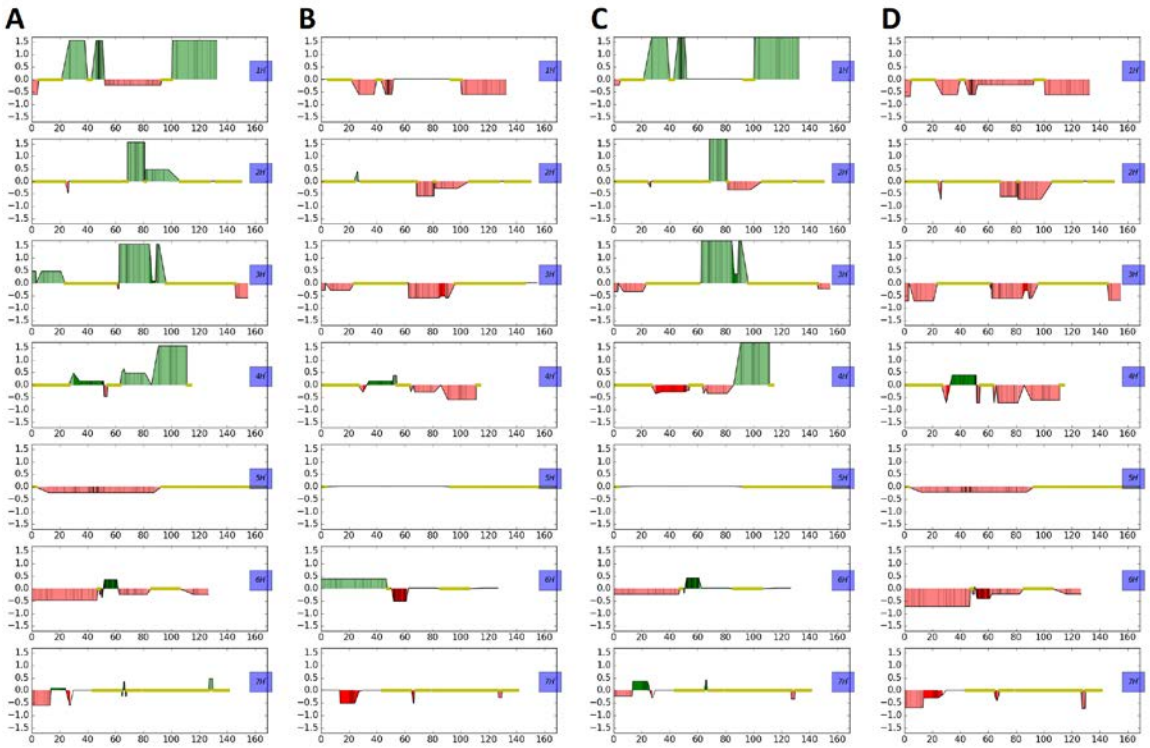

Figure 5. *Chromosome regions associated with root elongation rates. Green areas of the graph indicate region of the genome for which variations are associated with changes in the quantitative trait. Red areas of the graph indicate regions of the genome for which variations are not associated with variations in root traits. Darker regions (respectively green or red) indicate regions where there is more chromosomal introgression for which estimates are likely to be more*

accurate. Horizontal lines in yellow indicate region of the genome for which no genetic variations are observed within the selection of genotypes studied. Chromosome regions associated with primary elongation rate A), gravitropic rate B), lateral root elongation rate C), and branching rate D).

C-QTL analysis provided a coarse but extensive map of the influence of wild barley chromosomal introgression on rooting traits (Fig. 5-6). Because of the small number of genotypes studied, only a few substitution segments from the wild genome were tested and associations for several root growth parameters are likely to co-vary with other unrelated markers (Fig. 1D). Regions associated with primary and lateral root elongation rates (Fig. 5 A, C) were mostly identical across the genome, with the highest scores recorded simultaneously on chromosomes 1H, 2H, 3H and 4H, moderate score values on chromosome 6H and no associations on chromosome 5H. In addition, small groups of markers on chromosomes 2H, 3H, and 7H appear to be solely associated with the elongation rate of seminal roots whereas a common group of markers on chromosome 4H was found to overlap with seminal elongation rate, gravitropism and branching rate. In particular, the wild barley introgression on chromosome 2H (68.6cM to 80.9cM) found on OSU048 could be linked in elongation rate. Few QTLs have been reported in the literature for root growth rate parameters in barley (Gregory et al., 2009), while Chen et al. (2010) and (Arifuzzaman et al., 2014)detected genomic regions on chromosomes 2H, 3H and 5H influencing root length. Both authors used populations derived from Israeli wild barley accessions in their studies and showed the potential of the unadapted genome to contribute favourable alleles to increase root length and subsequent adaptation to water-limited environments.

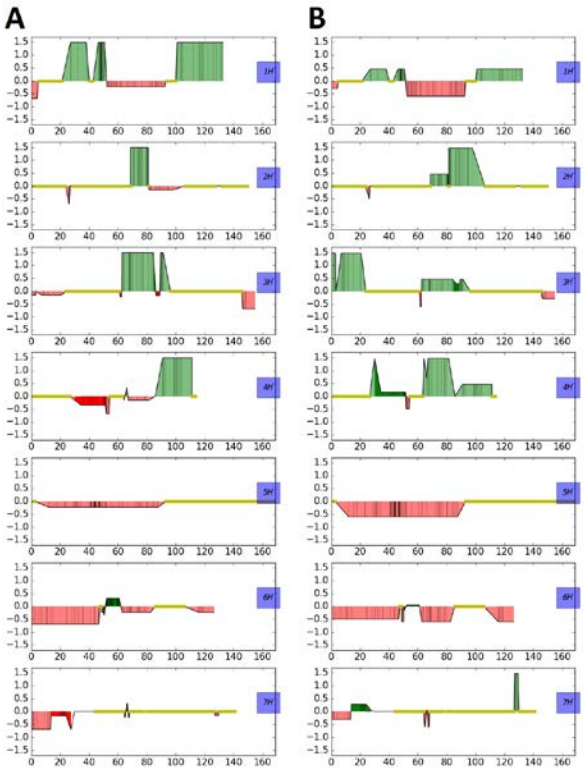

Figure 6. *Change in regions associated with primary elongation rate with time. Chromosome regions associated with primary elongation rate at day 10 A) and primary elongation rate at day 16 B) showed a few differences in chromosomes 2H, 3H, 4H and 7H.*

Regions associated with gravitropic rate (Fig. 5B) and branching rate (Fig. 5D) were less significant than the associations found for elongation rate of primary and lateral roots. Two regions on chromosome 2H and 6H were uniquely associated with gravitropic rate and a large group of markers chromosome 5H was found to be associated with the trait but with a very low score. Recently Robinson et al. (2016) reported a major QTL associated with root spread on chromosome 5H using a double haploid population (ND24260 X Flagship). The authors found this region collocated with other QTL controlling seminal root number which also mapped in the vicinity of aboveground quantitative traits related to drought adaptation in barley. A chromosomal region on 7H was associated solely with the elongation rate of lateral roots and a chromosomal region on 4H was associated only with the branching rate. No QTLs have been reported for this trait in previous studies. It is also interesting to note that the score of markers associated with the primary

678 elongation rate and the branching rate varied strongly as a function of time (Fig. 6), whereas the
679 score associated with the elongation rate of lateral roots was more consistent at the different time
680 steps.
681 Accurate identification of root QTL from a small subset of RCSL genotypes is challenging. First
682 results showed correlations exist between groups of markers because of limited number of
683 genotypic combinations within the genome (Fig. 1). Physiological interactions are also likely to
684 create natural correlations between several traits. It is often observed that elongation of primary
685 and lateral roots are linked; for example, enhanced elongation of lateral roots coincides with a
686 reduction in the growth of primary (Williamson et al., 2001). In order to overcome such
687 limitations, it is important therefore, to optimise the distribution of wild introgressions within a
688 selection of RCSL genotypes to be used in a study. An essential property to consider for the C-
689 QTL approach is the balance between wild and cultivated introgressions within the selection of
690 genotypes. An ideal set of lines would have introgressions arranged with minimum overlapping of
691 segments and each marker would appear in exactly the same number of times in the set of
692 genotypes. This is difficult to achieve practically because of the large number of genotypes that
693 would be required. For example, with 10 segments a full factorial set of introgressions would
694 require 210 to 1024 genotypes. A more straightforward and effective approach would be to
695 phenotype introgression lines harbouring a unique exotic insert from the donor parent genome.
696 Lines from the initial cross between cv. Scarlett X ISR42-8 (Von Korff et al., 2004) have been
697 further backcrossed to the recurrent parent and new subsets of lines with unique introgressions
698 have been used in root QTL mapping studies (Hoffmann et al., 2012; Naz et al., 2014). In this case,
699 QTLs are located to the target segment making the introgression line significantly different from
700 the donor parent and the results can be validated using a small number of introgression lines
701 (Ahmad Naz et al., 2012). However, this approach is not suitable for groups of introgresion lines in
702 earlier generations (BC2) since they contain several alien inserts in their genome. The C-QTL
703 approach could aid the selection of target regions putatively associated with the trait for further
704 experiments, optimising the number of introgression lines used and the backcross strategy to obtain
705 near isogenic lines and ultimately identify the genes underlying the QTL.

CONCLUSION

The speed and efficiency of root phenotyping is limiting the ability of research groups to map QTLs of root-related traits. The combined imaging and modelling pipeline developed in this paper allowed efficient measurement of root traits and potential identification of QTLs linked to root elongation, branching rate and gravitropism for both main axes and first order lateral roots in barley. The use of barley RCSLs with well-defined chromosomal introgressions enabled identification of QTLs of interest with relatively few lines in a time lapse dataset. The immediate next step is to design the next generation of RCSL lines and so better refine the chromosomal regions associated with root growth parameters. This general approach should be transportable between crop species and may be applicable in a wider range of growth systems where roots can be imaged, including root boxes where roots are grown in soil. As such, the proposed framework is a valuable step forward in advancing the range of methods available for root phenotyping, though further testing and verification will be needed for each new crop growth system adopted.

LIST OF SYMBOLS AND NOTATIONS

Growth Model

x,y	cm	Spatial coordinates
α		Root angle
t	d	time
e	cm· d^{-1}	Elongation rate
b_r	d^{-1}	Branching rate
b_a		Branching angle
g	d^{-1}	Gravitropic rate
n		Total root number
l	cm	Total root length
ρ_a	cm^{-2}	Root tip density
ρ_l	cm^{-1}	Root length density
T	d	Time delay for lateral root initiation
$\wedge$		Direct estimate of a model parameter on data
$()$		Number in superscript and in parentheses indicate the root branching order

Genetic analysis

G^i	genetic make-up of the i^{th} genotype
g_k^i	value of the k^{th} introgression of the i^{th} genotype. The value is 0 if the k^{th} marker is that of the elite line and 1 if the marker is that of the exotic line.
φ^i	phenotype of the i^{th} genotype represented as a scalar value, for example a root growth parameter
b_k	the genetic effect of the k^{th} introgression
$D_k^{1,2}$	positive contribution to the score of the k^{th} introgression determined from two subgroups of genotypes U_1 and U_2
E_k	negative contribution to the score of the k^{th} introgression
δ_k^{12}	genetic difference factor that indicates when two subgroups of genotypes (U_1 and U_2) segregates at loci k
γ_k^r	genetic difference factor that indicates when a subgroup of genotype (U_r) has variation at loci k

ACKNOWLEDGEMENT

Michael Adu provided invaluable help during the development of the experimental set up. We also thank Prof. X. Draye for useful discussions during the design of this work and Philip White for the valuable comments provided on the manuscript. This work was supported by the EU FP7 project EURoot 'Enhanced models for predicting RSA development under multiple stresses' (2011–2016, KBBE.2011.1.2-05 no 289300). The James Hutton Institute received support from the Scottish

Government Rural and Environment Science and Analytical Services Division (RESAS, Workpackage 2.1.7, 2.3.4)

REFERENCES

Adu, M. O., Chatot, A., Wiesel, L., Bennett, M. J., Broadley, M. R., White, P. J., Dupuy, L. X., 2014. A scanner system for high-resolution quantification of variation in root growth dynamics of *Brassica rapa* genotypes. J Exp Bot 54, 1431-1446, doi:10.1093/jxb/eru048.

Ahmad Naz, A., Ehl, A., Pillen, K., Léon, J., 2012. Validation for root-related quantitative trait locus effects of wild origin in the cultivated background of barley (*Hordeum vulgare* L.). Plant Breeding 131, 392-398.

Arai-Sanoh, Y., Takai, T., Yoshinaga, S., Nakano, H., Kojima, M., Sakakibara, H., Kondo, M., Uga, Y., 2014. Deep rooting conferred by DEEPER ROOTING 1 enhances rice yield in paddy fields. Sci Rep 4.

Araki, H., Morita, S., Tatsumi, J., Iijima, M., 2002. Physiol-morphological analysis on axile root growth in upland rice. Plant production science 5, 286-293.

Arifuzzaman, M., Sayed, M. A., Muzammil, S., Pillen, K., Schumann, H., Naz, A. A., Léon, J., 2014. Detection and validation of novel QTL for shoot and root traits in barley (Hordeum vulgare L.). Mol Breed 34, 1373-1387.

Armengaud, P., Zambaux, K., Hills, A., Sulpice, R., Pattison, R. J., Blatt, M. R., Amtmann, A., 2009. EZ-Rhizo: integrated software for the fast and accurate measurement of root system architecture. The Plant Journal 57, 945-956.

Atkinson, J. A., Wingen, L. U., Griffiths, M., Pound, M. P., Gaju, O., Foulkes, M. J., Le Gouis, J., Griffiths, S., Bennett, M. J., King, J., 2015. Phenotyping pipeline reveals major seedling root growth QTL in hexaploid wheat. J Exp Bot 66, 2281-2292.

Bengough, A. G., Gordon, D. C., Al-Menaie, H., Ellis, R. P., Allan, D., Keith, R., Thomas, W. T. B., Forster, B. P., 2004. Gel observation chamber for rapid screening of root traits in cereal seedlings. Plant Soil 262, 63-70.

Bingham, I. J., Bengough, A. G., Rees, R. M., 2010. Soil compaction–N interactions in barley: root growth and tissue composition. Soil and Tillage Research 106, 241-246.

Boserup, E., 2005. The conditions of agricultural growth: The economics of agrarian change under population pressure. Transaction Publishers.

Burman, P., 1989. A comparative study of ordinary cross-validation, v-fold cross-validation and the repeated learning-testing methods. Biometrika 76, 503-514.

765 Cai, G., Vanderborght, J., Klotzsche, A., van der Kruk, J., Neumann, J., Hermes, N., Vereecken,
766 H., 2016. Construction of Minirhizotron Facilities for Investigating Root Zone Processes.
767 Vadose Zone Journal 15.
768 Chen, G., Krugman, T., Fahima, T., Chen, K., Hu, Y., Röder, M., Nevo, E., Korol, A., 2010.
769 Chromosomal regions controlling seedling drought resistance in Israeli wild barley,
770 *Hordeum spontaneum* C. Koch. Genet Resour Crop Evol 57, 85-99.
771 Chloupek, O., Forster, B. P., Thomas, W. T., 2006. The effect of semi-dwarf genes on root system
772 size in field-grown barley. Theor Appl Genet 112, 779-786.
773 Clark, R. T., MacCurdy, R. B., Jung, J. K., Shaff, J. E., McCouch, S. R., Aneshansley, D. J.,
774 Kochian, L. V., 2011. Three-dimensional root phenotyping with a novel imaging and
775 software platform. Plant Physiol 156, 455-465.
776 Comas, L., Becker, S., Cruz, V. M. V., Byrne, P. F., Dierig, D. A., 2013. Root traits contributing to
777 plant productivity under drought. Frontiers in Plant Science 4,
778 doi:10.3389/fpls.2013.00442.
779 Courtois, B., Ahmadi, N., Khowaja, F., Price, A. H., Rami, J.-F., Frouin, J., Hamelin, C., Ruiz, M.,
780 2009. Rice root genetic architecture: meta-analysis from a drought QTL database. Rice 2,
781 115-128.
782 de Dorlodot, S., Forster, B., Pagès, L., Price, A., Tuberose, R., Draye, X., 2007. Root system
783 architecture: opportunities and constraints for genetic improvement of crops. Trends Plant
784 Sci 12, 474-481.
785 de la Fuete Canto, C., 2016. Recombinant Chromosome Substitution Lines as a source of genetic
786 variation for drought stress tolerance in barley Vol. PhD. University of Dundee.
787 de la Fuete Canto, C., 2018. Test data for C-QTL analysis of barley Recombinant Chromosome
788 Substitution Lines. https://doi.org/10.5281/zenodo.1196298.
789 Del Pozo, A., Castillo, D., Inostroza, L., Matus, I., Méndez, A., Morcuende, R., 2012.
790 Physiological and yield responses of recombinant chromosome substitution lines of barley
791 to terminal drought in a Mediterranean-type environment. Ann Appl Biol 160, 157-167.
792 do Rosario, M., Oliveira, G., Van Noordwijk, M., Gaze, S. R., Brouwer, G., Bona, S., Mosca, G.,
793 Hairiah, K., 2000. Auger sampling, ingrowth cores and pinboard methods. In: Smit, A., et
794 al., Eds.), Root method a handbook. Springer, Berlin.
795 Doerge, R. W., Churchill, G. A., 1996. Permutation tests for multiple loci affecting a quantitative
796 character. Genetics 142, 285-294.
797 Downie, H., Holden, N., Otten, W., Spiers, A. J., Valentine, T. A., Dupuy, L. X., 2012.
798 Transparent soil for imaging the rhizosphere. PLoS One 7, e44276.
799 Downie, H., Adu, M., Schmidt, S., Otten, W., Dupuy, L., White, P., Valentine, T., 2015.
800 Challenges and opportunities for quantifying roots and rhizosphere interactions through
801 imaging and image analysis. Plant, Cell Environ 38, 1213-1232.

802 Dupuy, L. X., Vignes, M., McKenzie, B., White, P., 2010. The dynamics of root meristem
803 distribution in soil. Plant, Cell Environ 33, 358-369.
804 Efron, B., Tibshirani, R. J., 1994. An introduction to the bootstrap. CRC press.
805 Forde, B., Lorenzo, H., 2001. The nutritional control of root development. Plant Soil 232, 51-68.
806 Forde, B. G., 2009. Is it good noise? The role of developmental instability in the shaping of a root
807 system. J Exp Bot 60, 3989-4002.
808 Garré, S., Laloy, E., Javaux, M., Vereecken, H., 2012. Parameterizing a dynamic architectural
809 model of the root system of spring barley from minirhizotron data. Vadose Zone Journal
810 11.
811 Geldermann, H., Pieper, U., Roth, B., 1985. Effects of marked chromosome sections on milk
812 performance in cattle. Theor Appl Genet 70, 138-146.
813 Gioia, T., Galinski, A., Lenz, H., Müller, C., Lentz, J., Heinz, K., Briese, C., Putz, A., Fiorani, F.,
814 Watt, M., 2017. GrowScreen-PaGe, a non-invasive, high-throughput phenotyping system
815 based on germination paper to quantify crop phenotypic diversity and plasticity of root
816 traits under varying nutrient supply. Funct Plant Biol 44, 76-93.
817 Gregory, P. J., Bengough, A. G., Grinev, D., Schmidt, S., Thomas, W. T. B., Wojciechowski, T.,
818 Young, I. M., 2009. Root phenomics of crops: opportunities and challenges. Funct Plant
819 Biol 36, 922-929, doi:doi:10.1071/FP09150.
820 Hackett, C., Rose, D., 1972. A model of the extension and branching of a seminal root of barley,
821 and its use in studying relations between root dimensions. 1. The model. Australian Journal
822 of Biological Science 25, 669-679.
823 Heinen, M., Mollier, A., De Willigen, P., 2003. Growth of a root system described as diffusion. 2.
824 Numerical model and application. Plant Soil 252, 251-265.
825 Hoffmann, A., Maurer, A., Pillen, K., 2012. Detection of nitrogen deficiency QTL in juvenile wild
826 barley introgression linesgrowing in a hydroponic system. BMC Genet 13, 88.
827 Hund, A., Ruta, N., Liedgens, M., 2009. Rooting depth and water use efficiency of tropical maize
828 inbred lines, differing in drought tolerance. Plant Soil 318, 311-325.
829 Kalogiros, D. I., Adu, M. O., White, P. J., Broadley, M. R., Draye, X., Ptashnyk, M., Bengough, A.
830 G., Dupuy, L. X., 2016. Analysis of root growth from a phenotyping data set using a
831 density-based model. J Exp Bot 67, 1045-1058, doi:10.1093/jxb/erv573.
832 Kato, Y., Abe, J., Kamoshita, A., Yamagishi, J., 2006. Genotypic variation in root growth angle in
833 rice (Oryza sativa L.) and its association with deep root development in upland fields with
834 different water regimes. Plant Soil 287, 117-129.
835 Kim, H. J., Fay, M. P., Feuer, E. J., Midthune, D. N., 2000. Permutation tests for joinpoint
836 regression with applications to cancer rates. Stat Med 19, 335-351.
837 Kristensen, H. L., Thorup-Kristensen, K., 2004. Root growth and nitrate uptake of three different
838 catch crops in deep soil layers. Soil Sci Soc Am J 68, 529-537.

839 Kumar, P., Huang, C., Cai, J., Miklavcic, S. J., 2014. Root phenotyping by root tip detection and
840 classification through statistical learning. Plant Soil 380, 193-209.
841 Lambers, H., Shane, M. W., Cramer, M. D., Pearse, S. J., Veneklaas, E. J., 2006. Root structure
842 and functioning for efficient acquisition of phosphorus: matching morphological and
843 physiological traits. Ann Bot 98, 693-713.
844 Le Marié, C., Kirchgessner, N., Marschall, D., Walter, A., Hund, A., 2014. Rhizoslides: paper-
845 based growth system for non-destructive, high throughput phenotyping of root
846 development by means of image analysis. Plant Methods 10, 1.
847 Leitner, D., Felderer, B., Vontobel, P., Schnepf, A., 2014. Recovering root system traits using
848 image analysis exemplified by two-dimensional neutron radiography images of lupine.
849 Plant Physiol 164, 24-35.
850 Letter, D., Seidel, R., Liebhardt, W., 2003. The performance of organic and conventional cropping
851 systems in an extreme climate year. Am J Alternative Agric 18, 146-154.
852 Liao, H., Rubio, G., Yan, X., Cao, A., Brown, K. M., Lynch, J. P., 2001. Effect of phosphorus
853 availability on basal root shallowness in common bean. Plant Soil 232, 69-79.
854 Lobet, G., Pagès, L., Draye, X., 2011. A novel image-analysis toolbox enabling quantitative
855 analysis of root system architecture. Plant Physiol 157, 29-39.
856 Lynch, J., Brown, K., 2002. Topsoil foraging - an architectural adaptation of plants to low
857 phosphorus availability. Plant Soil 237, 225-237.
858 Lynch, J. P., 2011. Root phenes for enhanced soil exploration and phosphorus acquisition: tools for
859 future crops. Plant Physiol 156, 1041-1049, doi:10.1104/pp.111.175414.
860 Mairhofer, S., Zappala, S., Tracy, S. R., Sturrock, C., Bennett, M., Mooney, S. J., Pridmore, T.,
861 2012. RooTrak: automated recovery of three-dimensional plant root architecture in soil
862 from X-ray microcomputed tomography images using visual tracking. Plant Physiol 158,
863 561-569.
864 Makowski, P., Sorensen, T. S., Therkildsen, S. V., Materka, A., Stodkilde-Jorgensen, H., Pedersen,
865 E. M., 2002. Two-phase active contour method for semiautomatic segmentation of the
866 heart and blood vessels from MRI images for 3D visualization. Comput Med Imaging
867 Graph 26, 9-17.
868 Matus, I., Corey, A., Filichkin, T., Hayes, P., Vales, M., Kling, J., Riera-Lizarazu, O., Sato, K.,
869 Powell, W., Waugh, R., 2003. Development and characterization of recombinant
870 chromosome substitution lines (RCSLs) using *Hordeum vulgare* subsp. spontaneum as a
871 source of donor alleles in a Hordeum vulgare subsp. vulgare background. Genome 46,
872 1010-1023.
873 Mooney, S., Pridmore, T., Helliwell, J., Bennett, M., 2012. Developing X-ray computed
874 tomography to non-invasively image 3-D root systems architecture in soil. Plant Soil 352,
875 1-22.

Nagel, K. A., Putz, A., Gilmer, F., Heinz, K., Fischbach, A., Pfeifer, J., Faget, M., Blossfeld, S., Ernst, M., Dimaki, C., 2012. GROWSCREEN-Rhizo is a novel phenotyping robot enabling simultaneous measurements of root and shoot growth for plants grown in soil-filled rhizotrons. Funct Plant Biol 39, 891-904.

Naz, A. A., Arifuzzaman, M., Muzammil, S., Pillen, K., Léon, J., 2014. Wild barley introgression lines revealed novel QTL alleles for root and related shoot traits in the cultivated barley (Hordeum vulgare L.). BMC Genet 15, 107.

Pedregosa, F., Varoquaux, G., Gramfort, A., Michel, V., Thirion, B., Grisel, O., Blondel, M., Prettenhofer, P., Weiss, R., Dubourg, V., 2011. Scikit-learn: Machine learning in Python. The Journal of Machine Learning Research 12, 2825-2830.

Pound, M. P., French, A. P., Atkinson, J. A., Wells, D. M., Bennett, M. J., Pridmore, T., 2013. RootNav: navigating images of complex root architectures. Plant Physiol 162, 1802-1814.

Reddy, V. R., Pachepsky, Y. A., 2001. Testing a convective-dispersive model of two-dimensional root growth and proliferation in a greenhouse experiment with maize plants. Ann Bot 87, 759-768.

Rewald, B., Ephrath, J. E., 2012. Minirhizotron technique. Plant roots: the hidden half, 4th edn. CRC Press, New York.

Robinson, H., Hickey, L., Richard, C., Mace, E., Kelly, A., Borrell, A., Franckowiak, J., Fox, G., 2016. Genomic regions influencing seminal root traits in barley. The Plant Genome 9.

Rose, D., 1983. The description of the growth of root systems. Plant Soil 75, 405-415.

Sandhu, N., Kumar, A., 2017. Bridging the rice yield gaps under Drought: QTLs, genes, and their use in breeding programs. Agronomy 7, 27.

Schindelin, J., Arganda-Carreras, I., Frise, E., Kaynig, V., Longair, M., Pietzsch, T., Preibisch, S., Rueden, C., Saalfeld, S., Schmid, B., 2012. Fiji: an open-source platform for biological-image analysis. Nat Methods 9, 676-682.

Secchi, S., Gassman, P. W., Jha, M., Kurkalova, L., Feng, H. H., Campbell, T., Kling, C. L., 2007. The cost of cleaner water: assessing agricultural pollution reduction at the watershed scale. Journal of Soil and Water Conservation 62, 10-21.

Shelden, M. C., Roessner, U., Sharp, R. E., Tester, M., Bacic, A., 2013. Genetic variation in the root growth response of barley genotypes to salinity stress. Funct Plant Biol 40, 516-530.

Tambussi, E., Bort, J., Araus, J., 2007. Water use efficiency in C3 cereals under Mediterranean conditions: a review of physiological aspects. Ann Appl Biol 150, 307-321.

Thomas, C., Graham, N., Hayden, R., Meacham, M., Neugebauer, K., Nightingale, M., Dupuy, L., Hammond, J., White, P., Broadley, M., 2016. High-throughput phenotyping (HTP) identifies seedling root traits linked to variation in seed yield and nutrient capture in field-grown oilseed rape (*Brassica napus* L.). Ann Bot 118, 655-665.

912 Topp, C. N., Iyer-Pascuzzi, A. S., Anderson, J. T., Lee, C.-R., Zurek, P. R., Symonova, O., Zheng,
913 Y., Bucksch, A., Mileyko, Y., Galkovskyi, T., 2013. 3D phenotyping and quantitative trait
914 locus mapping identify core regions of the rice genome controlling root architecture.
915 Proceedings of the National Academy of Sciences 110, E1695-E1704.
916 Trachsel, S., Kaeppler, S. M., Brown, K. M., Lynch, J. P., 2011. Shovelomics: high throughput
917 phenotyping of maize (*Zea mays* L.) root architecture in the field. Plant Soil 341, 75-87.
918 Uga, Y., Sugimoto, K., Ogawa, S., Rane, J., Ishitani, M., Hara, N., Kitomi, Y., Inukai, Y., Ono, K.,
919 Kanno, N., 2013. Control of root system architecture by DEEPER ROOTING 1 increases
920 rice yield under drought conditions. Nat Genet 45, 1097-1102.
921 Valentine, T. A., Hallett, P. D., Binnie, K., Young, M. W., Squire, G. R., Hawes, C., Bengough, A.
922 G., 2012. Soil strength and macropore volume limit root elongation rates in many UK
923 agricultural soils. Ann Bot 110, 259-270, doi:10.1093/aob/mcs118.
924 Von Korff, M., Wang, H., Léon, J., Pillen, K., 2004. Development of candidate introgression lines
925 using an exotic barley accession (*Hordeum vulgare* ssp. spontaneum) as donor. Theor Appl
926 Genet 109, 1736-1745.
927 Watt, M., Kirkegaard, J. A., Rebetzke, G. J., 2005. A wheat genotype developed for rapid leaf
928 growth copes well with the physical and biological constraints of unploughed soil. Funct
929 Plant Biol 32, 695-706.
930 White, P. J., Broadley, M. R., Gregory, P. J., 2012. Managing the nutrition of plants and people.
931 Applied and Environmental Soil Science 2012, 104826.
932 White, P. J., George, T. S., Gregory, P. J., Bengough, A. G., Hallett, P. D., McKenzie, B. M., 2013.
933 Matching roots to their environment. Ann Bot 112, 207-222.
934 Wilkinson, S., Davies, W. J., 2002. ABA-based chemical signalling: the co-ordination of responses
935 to stress in plants. Plant Cell and Environment 25, 195-210.
936 Williamson, L. C., Ribrioux, S. P., Fitter, A. H., Leyser, H. O., 2001. Phosphate availability
937 regulates root system architecture in Arabidopsis. Plant Physiol 126, 875-882.
938